Spatiotemporal Patterns and Nonclassical Kinetics of Competing Elementary Reactions: Chromium Complex Formation with Xylenol Orange in a Capillary

Andrew Yen,[†] Anna L. Lin,[†] Yong-Eun Lee Koo,[†,‡] Baruch Vilensky,[§] Haim Taitelbaum,[§] and Raoul Kopelman*[,†,§]

Department of Chemistry, University of Michigan, Ann Arbor, Michigan 48109-1055, and Department of Physics, Bar-Ilan University, Ramat-Gan 52900, Israel

Received: September 27, 1996; In Final Form: January 3, 1997[⊗]

An experimental investigation of chemical reaction fronts, created by an initial separation of reactants, is reported for a system of two competing reactions. Spatiotemporal patterns are observed experimentally for the competing reaction front and are accounted for quantitatively by a reaction-diffusion model. We use the reaction of xylenol orange with Cr^{3+} in aqueous solution. Different oligomers of Cr^{3+} provide the two kinetically different species that react competitively with xylenol orange. The parameters that determine whether pattern formation is observable at the front are the ratios of (1) the microscopic reaction constants of the competing reactions and (2) the concentrations of the competing species. Under the parameter values studied, which allowed clear spatiotemporal separation of the two competing reactions, we find that the behavior of the reaction front at *early* times follows a perturbation theory developed for a simple elementary A + B → C reaction with initially separated reactants. The global reaction rate, observed over the entire time scale of the experiments, is highly non-monotonic. Overall, with no free parameters, our theoretical model is quantitatively consistent with the experimental observations of the spatiotemporal patterns, the unusual scaling laws, and the crossover behaviors. The geometrical constraints and nonclassical behavior of the reaction rate allow a quantitative determination of the reaction probability of the chromium ion monomer relative to that of the higher order oligomers.

I. Introduction

Chemical reaction fronts generated as a result of far from equilibrium physicochemical conditions and processes are common in nature.[1,2] Examples of chemical reaction fronts[3] generated in the laboratory are Liesegang rings[4,5] and traveling chemical waves, such as those seen in the Belousov−Zhabotinskii[6−9] reaction. The formation of traveling chemical waves involves, among other factors, competition among some of the reagents for reaction with one another. The overall reaction mechanism is usually quite complex.

The simplest forms of chemical reaction fronts have been investigated in a series of recent theoretical and experimental papers.[10−37] It has been shown that, even for a single bimolecular reaction, elementary reaction-diffusion systems with initially separated reactants can exhibit very unusual dynamic properties. The latter includes the global reaction rate, $R(t)$, the location of the center of the reaction front, $x_f(t)$, the width of the front, $w(t)$, and the rate of reaction at the center of the front, $R(x_f,t)$.

We present here results obtained from an experimental and theoretical investigation of a slightly more complex reaction front, one in which there are two competing chemical reactions. We create a chemical reaction front in a capillary under the condition of initially separated reactants and report the first experimental observation of a crossover in the scaling of the width, from $t^{1/2}$ at early time to $t^{1/6}$ asymptotically, and of the global rate, from $t^{1/2}$ at early time to $t^{-1/2}$ asymptotically, as predicted by perturbation analysis[13] for the simple A + B → C reaction. Subsequently, we observe a splitting of the chemical reaction front in space. The latter occurs as the second competing reaction starts to dominate the kinetics. The resulting dynamic patterns in both real and reaction space are accounted for by our model. The low-dimensional experimental setup together with the nonclassical rate laws enable us to extract the relative reaction probabilities of the chromium ion monomer and its higher oligomers.

II. Theoretical Framework for the Kinetics of a Reaction Front

The first theoretical work on the reaction-diffusion system with initially separated components was done by Galfi and Racz[10] on the irreversible A + B → C reaction, for which they predicted the *asymptotic* behavior of the reaction front. In their reaction model, reactant A, with concentration a_0, and reactant B, with concentration b_0, are initially separated. They meet at time 0, forming a reaction front. The initially separated condition makes the system effectively one-dimensional. Experimentally it is implied that the tube is homogeneously filled with an inert, convectionless solvent.[11]

The following set of mean-field type reaction-diffusion equations for the local concentrations a, b has been assumed to describe the system[10]

$$\frac{\partial a}{\partial t} = D_a \nabla^2 a - kab$$

$$\frac{\partial b}{\partial t} = D_b \nabla^2 b - kab \qquad (1)$$

where D_a and D_b are the diffusion coefficients and k is the microscopic reaction constant. The equations are subject to the

[†] University of Michigan.
[‡] Present address: Inorganic Division, Department of Chemistry, National Institute of Technology and Quality, 2 Chungang-dong, Kwachon, Kyounggido, Korea.
[§] Bar-Ilan University.
* Corresponding author.
[⊗] Abstract published in *Advance ACS Abstracts,* March 15, 1997.

S1089-5639(96)02994-5 CCC: $14.00

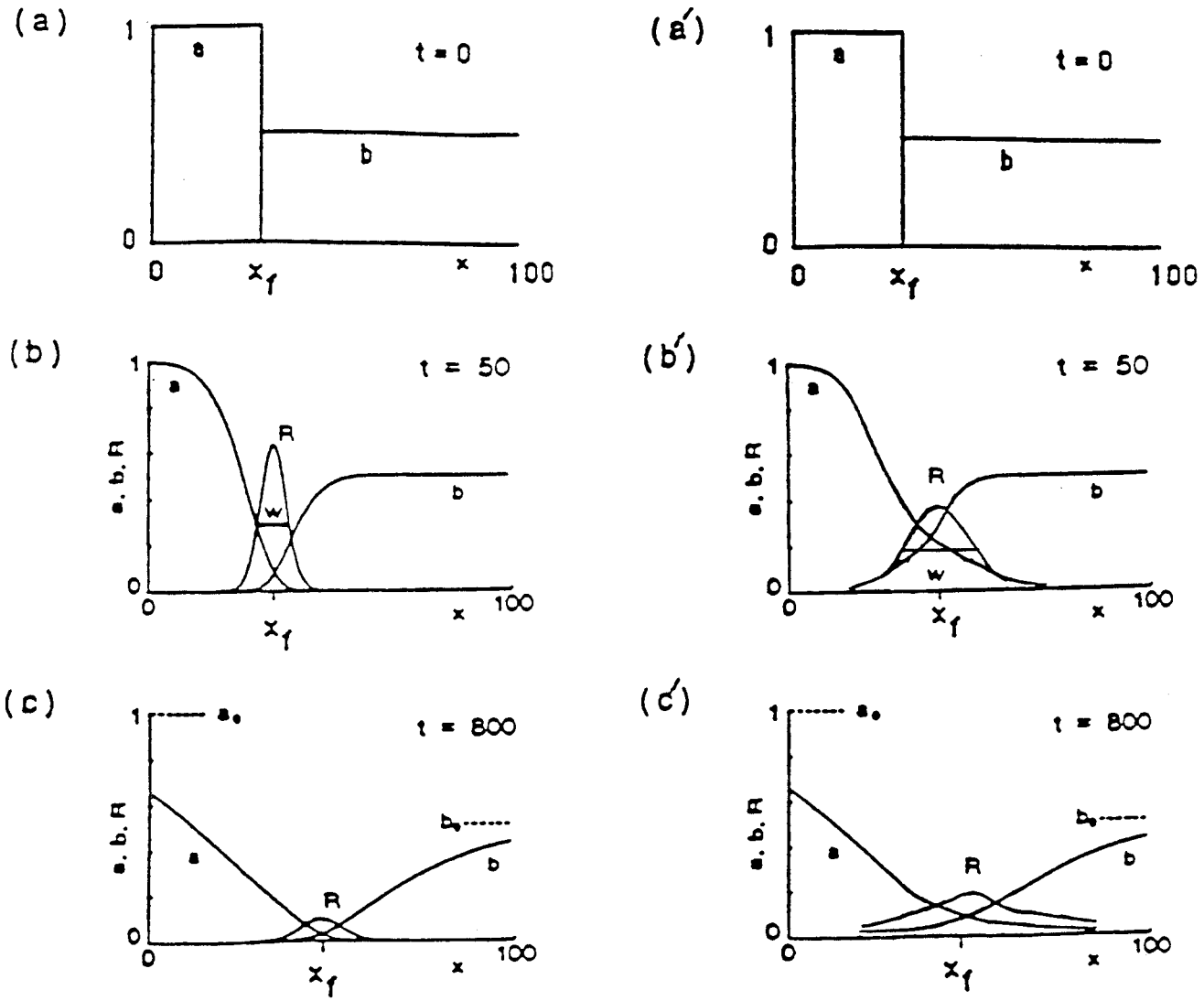

Figure 1. Schematic diagrams of diffusion-limited (left column) and reaction-limited (right column) chemical reaction fronts. The curves labeled a and b denote the relative concentrations of reactants A and B. Here *R* denotes the magnified production rate of C, while *w* denotes the width of the reaction front.

initial separation condition along the separation axis, *x*

$$a = a_0[1 - H(x)] \qquad b = b_0H(x) \tag{2}$$

where a_0 and b_0 are the initial concentrations and $H(x)$ is the Heaviside step function. Their study shows that when $a_0 \neq b_0$ and $D_a = D_b$ the position of the center of the reaction front (x_f) and the width (w) of the front scale with time, as $x_f \sim t^{1/2}$ and $w \sim t^{1/6}$, respectively, while the local production rate of C at x_f is proportional to $t^{-2/3}$, in the asymptotic regime. The global rate, $R(t)$, which is defined as the integral of the local rate over space, scales as $t^{-1/2}$ asymptotically. These results are different from the classical predictions ($x_f \sim$ *constant*, $w \sim t^{1/2}$, $R(x_f,t) \sim$ *constant*, $R(t) \sim t^{1/2}$). This system has been studied experimentally, and the experimental results are in good agreement with the theory.[10,33]

The early time behavior of this irreversible A + B → C system was studied theoretically by Taitelbaum et al.[13] It was found that $R(t)$ and $w(t)$ exhibited a crossover at early time, from the classical behavior to the anomalous behavior: $R(t) \sim t^{1/2}$ to $R(t) \sim t^{-1/2}$ and $w(t) \sim t^{1/2}$ to $w(t) \sim t^{1/6}$. The reaction-limited early time behavior and the diffusion-limited asymptotic behavior are shown schematically in Figure 1.

The case of two competing reactions is the first stage of complexity beyond the model of simple, independently acting elementary reactions. We model such a system on the basis of the existence of two species on one side of the initially separated system. The two species, A_1 and A_2, which do not react with each other, are on one side of the system while the species B, which reacts with both A_1 and A_2, is on the other side. The reaction scheme is represented as

$$A_1 + B \rightarrow C_1 \tag{3a}$$

$$A_2 + B \rightarrow C_2 \tag{3b}$$

where 3a and 3b take place simultaneously. Thus, A_1 and A_2 compete to react with B. The products, C_1 and C_2, are assumed to be either identical or experimentally indistinguishable, and thus the local reaction rate of the system can be written as:

$$R(x,t) = k_1\rho_{a1}(x,t)\,\rho_b(x,t) + k_2\rho_{a2}(x,t)\,\rho_b(x,t) \tag{4}$$

We studied this model by computer simulation. Under conditions where k_1 exceeds k_2 by several orders of magnitude, and where the faster reacting A_1 species is only a small fraction of the total density of A ($A = A_1 + A_2$), the simulation shows that the reaction front consists of two distinguishable peaks and the global reaction rate is nonmonotonic in time, eventually

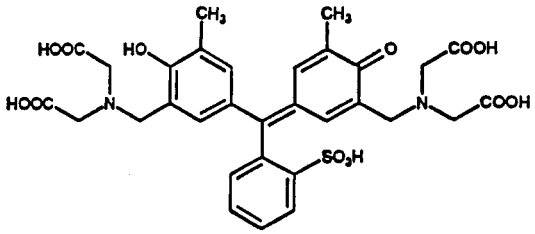

Figure 2. Structure of xylenol orange.

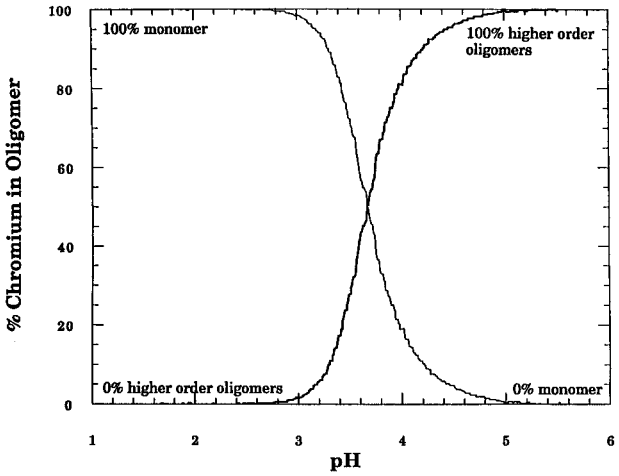

Figure 3. Percentage of Cr^{3+} monomers and higher order oligomers as a function of the pH of the solution. At pH = 4.5 the chromium solution consists of 3% monomer and 97% higher order oligomers. After Stunzi et al. (ref 38).

decreasing asymptotically as $t^{-1/2}$, the same as the asymptotic behavior exhibited for the simple A + B → C elementary reaction.

III. Chemical Considerations

We chose the following reactions[38−41] for our experiment:

$$Cr^{3+}(\text{monomer}) + \text{xylenol orange} \rightarrow \text{product} \quad (5a)$$

$$Cr^{3+}(\text{h.o. oligomer}) + \text{xylenol orange} \rightarrow \text{product} \quad (5b)$$

For the structure of xylenol orange (XO), see Figure 2. As the source of Cr^{3+} and XO we used $CrCl_3$ and the sodium salt of xylenol orange, respectively. There were several reasons for choosing these as our system of two competing reactions. (1) We need highly irreversible reactions that allow us to study the chemical reaction front under far from equilibrium conditions. (2) We also require two slow, reaction-limited reactions that compete with each other.

Reactive species of Cr^{3+} present in aqueous solution have been shown to be highly dependent on pH. Stunzi et al. studied the polymerization of Cr^{3+} in aqueous solution.[38] In their work they followed a 4 yr evolution of aqueous Cr^{3+} solutions at room temperature. While the different species of Cr^{3+} present in solution are very dynamic over this 4 yr period, our experiments occur over a period of hours, a time scale on which the composition of the solution is relatively constant (we first boil the reactants for 5 min, so as to speed up the equilibration process). The Cr^{3+} ions bind with H_2O, $-OH$, and other Cr^{3+} ions in solution to form monomeric, dimeric, and higher order (h.o.) oligomeric species of Cr^{3+}. At pH 4.5, approximately 3% of the Cr^{3+} in aqueous solution is in monomeric form and approximately 97% is in the form of higher order oligomers (Figure 3). We believe that the monomeric form of Cr^{3+} plays the role of the fast-reacting, low-concentration species, A_1 of the theoretical model, and the higher order oligomers together constitute the slow-reacting, high-concentration species, A_2 of the model. We expected the microscopic rate constant of the monomer to be higher than that of the higher order oligomers because the monomer is less sterically hindered (also, see discussion below).

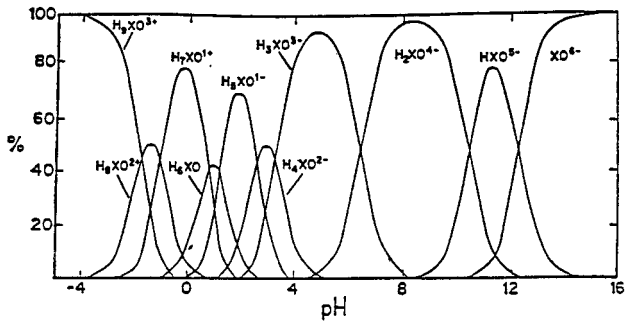

Figure 4. Percentage of 10 possible ionic forms of xylenol orange in aqueous solution as a function of pH. After Rehak and Korbl (ref 40).

Xylenol orange (XO) has 10 possible ionic forms[40] in aqueous solution (Figure 4). Which of these forms are present in solution, and in what ratio they are present, also depends on pH. The question was whether one can disregard XO as a possible source of the competing A_1 and A_2 species that causes a splitting of the reaction front. We conducted a series of "test tube" experiments, the results of which allowed us to disregard XO as the source of the A_1 and A_2 reactive species. Details of these experiments are given below.

Reacting Cr^{3+} with XO at pH 4.5, we expected to be able to observe the predicted spatiotemporal patterns because the two necessary criteria were met: the concentrations of the two A_i species (supplied by Cr^{3+}(aq)), as well as their microscopic rate constants for reaction with B, differ by orders of magnitude in the right direction. Because the microscopic rate constants of these two competing reactions differ by orders of magnitude it was also possible to observe with this reaction the early time behavior predicted by perturbation theory as well as to see the asymptotic behavior predicted by Galfi and Racz.

We performed these experiments in a gelatin solution. Besides deterring convection, the polymeric gelatin structure has many dangling $-O^{-}\cdots H^{+}$ functional groups that effectively shield the Cr^{3+} and XO reactant ions, thus preventing long range Coulombic interactions among the reactants.[42] The latter are also shielded by the counterions, Cl^{-} and Na^{+}.

IV. Experimental and Simulation Methods

a. Homogeneous Reaction Kinetics. Solutions of XO and Cr^{3+} with concentrations of 7.5×10^{-5} M Cr^{3+} and 5.0×10^{-4} M XO, and with a 0.8% wt:wt concentration of Ficoll and of Gelatin, were mixed together in a round bottom flask, creating a *homogeneous* reaction mixture. The $CrCl_3$ and the xylenol orange Na salt were purchased from Aldrich and were used without further purification. The gelatin and the Ficoll were purchased from Sigma. The pH values of the reactant solutions were buffered at either pH 4.0 or 4.5 with acetate buffer prior to mixing. After the two reagent solutions were mixed, the pH was measured again and it was determined to be the same as the pH of the individual reactant solutions from which it was created. For comparison, the same experiments were done using Co^{3+} and XO as the reactants. Hexaaminecolbalt(III) chloride was used as the source of Co^{3+} and was purchased from Strem Chemicals.

The different Cr^{3+} reactant species are transparent in the range of 280−750 nm, and the different product species could not be

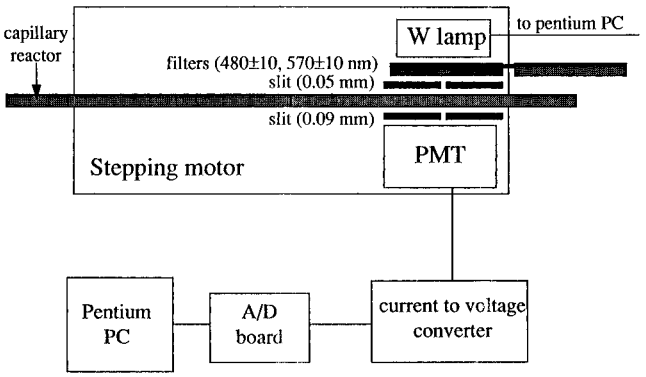

Figure 5. Schematic diagram of the experimental setup for the optical absorbance measurements along the reaction front.

distinguished with optical absorbance methods (neither could the different ionic forms of XO). Also, the different species of Cr^{3+} in our homogeneous reaction mixture are not separable: they exist in a quasi-equilibrium, and their ratio depends on the pH of the solution. However, we do obtain the relative rates of reaction of the homogeneous reaction mixtures at different pH values. The unreacted reactant mixture has a λ_{max} = 440 nm (yellow) optical absorbance due to the XO, and both product species[41] formed have a λ_{max} = 550 nm (purple) optical absorbance. Reactant solutions with a larger ratio of faster/slower reacting Cr^{3+} species transform from a yellow to a purple color distinguishably more rapidly than reactant solutions with a smaller ratio of faster/slower reacting Cr^{3+} species. The relative reaction rates of reactant mixtures buffered at pH 4.0 and 4.5 were monitored. The relative rate of reaction was monitored at 100 and at 22 °C.

b. Reaction Front Kinetics. *Sample preparation.* Aqueous solutions of Cr^{3+} and the XO were prepared with the appropriate concentrations of reagent, gelatin, and Ficoll. Two different sets of data are reported in this paper: one set of data is obtained using reagent solutions with concentrations of 7.5×10^{-5} M Cr^{3+} and 5.0×10^{-4} M XO, with a 0.8% wt:wt concentration of Ficoll and of gelatin, and the other set of data is obtained using reagent solutions with concentrations of 1.05×10^{-3} M Cr^{3+} and 1.10×10^{-4} M XO, with a 0.76% wt:wt concentration of Ficoll and of gelatin. The pH values of both reactant solutions were adjusted to 4.5 with acetate buffer, and the solutions were boiled. The samples were frozen and then stored in a refrigerator. Samples were allowed to equilibrate at room temperature before the experiments were run. Gelatin and the freezing process increase the viscosity of the reactant solutions, which prevents convection, and thus makes observation of the reaction front possible. Ficoll was added to fight fungal growth.

Reactor. We used a horizontal reactor, rather than the vertical reactors[44] used to measure diffusion coefficients in the 1930s and 1940s, and thus removed gravity as an experimental parameter in our system. The glass reactor is a rectangular tube (4×2 mm i.d.). A hole drilled in the center of the top wall acts as a pressure outlet.

Apparatus. Optical absorbance measurements were used to monitor the dynamic properties of the reaction front. The absorbance profiles of the product formation along the length of the tube were obtained by scanning along a defined length of the reactor, slits, and lamp in parallel with the rest of the detector (see experimental setup, Figure 5). The detection system consists of a halogen lamp, a solenoid with two filters, a slit unit, a stepping motor, and a PMT. The output of the PMT was sent through an A/D board to a pentium computer. The resulting digitized signal contained significant noise. To reduce this noise, we added a low-pass filter and averaged the signal at each data point . Details of the apparatus used to obtain spatitally resolved optical absorbance measurements are detailed elsewhere.[11]

Procedure. The reactants were injected into the ends of the reactor using two syringes. They met at the center of the reactor at time 0 and formed a vertical boundary. The first scan along the reaction front started when the reactants met. The time intervals between scans increased from the order of 1 min to the order of 100 min. Scans of the reaction front were taken in pairs—for each time interval, one scan of the product profile and one scan of the reactant profile were obtained. The lamp was turned on 4 min before each set of scans, to allow its output to stabilize.

Data Analysis. The optical absorbance of the total accumulated reaction product versus position, $A(x,t)$ vs x, was measured over time intervals that increased with time. Scans took 3 s to complete, and the interval between scans was on the order of minutes to hours. The Beer−Lambert law is valid over the concentration range of our experiments. Subtracting consecutive files gives ($A(x,t_2)$ vs x) − ($A(x,t_1)$ vs x) = $\Delta A(x,\Delta t)$ vs x. These subtraction profiles give the spatial distribution of product formation between time t and $t + \Delta t$. Normalizing by the proper time intervals, one obtains information equivalent to $R(x,t)$ vs position, x. From the $\Delta A(x,\Delta t)$ vs x profiles, we determined the time exponents for the dynamic properties of the reaction front.

The center of the reaction front was measured as the points with the highest values on the $\Delta A(x,\Delta t)$ vs x profiles. The reaction front width was measured at the half-height of each $\Delta A(x,\Delta t)$ vs x profile. The global rate was determined experimentally by dividing the base line corrected integrated area of the $\Delta A(x,\Delta t)$ vs x absorbance peaks by the appropriate time intervals, resulting in $\Delta A/\Delta t$ vs x plots.

c. Reaction Front Simulations. We studied this system via a simulation method based on a discrete version of the evolution equation.[34] At each time unit, n, all species perform a discrete diffusion step, using the exact enumeration method, followed by reaction events according to eq 1. Finite probabilities of reaction replace the reaction constants k_1 and k_2. We have assumed equal diffusion coefficients for all species and have studied a wide range of microscopic reaction constants and different fractions of the A_i's density out of the total A density.

V. Results

a. Homogenous Reaction Kinetics. In aqueous solutions containing both XO and Cr^{3+}, the overall rate of reaction, measured as total product accumulation, occurs faster at pH 4.0 than at pH 4.5. The purpose of these experiments was to determine which reactant, Cr^{3+} or XO, is the source of the A_i species. Since the chemistry of both Cr^{3+} and XO in aqueous solution depends on pH, this was done by determining the effect of pH on the relative overall reaction rate of the system.

Note that if our reaction scheme is to be consistent with the proposed model, then the *minority* species, A_1, must be the *"fast"* reacting species and the *majority* species, A_2, must be the *"slow"* reacting species. If XO is the source of A_1 and A_2, then A_1 must be the H_4XO^{2-} species and A_2 must be the H_3XO^{3-} species of XO, since H_3XO^{3-} exists in much excess of H_4XO^{2-} at pH 4.0−4.5 (see Figure 4). On the basis of general chemical arguments, which state that more highly charged ionic species react more quickly than those ions of the same species with lower charge,[45] there is a fast majority and a slow minority component, in contradiction to the model. Also, the reaction should occur more quickly at pH 4.5. (This

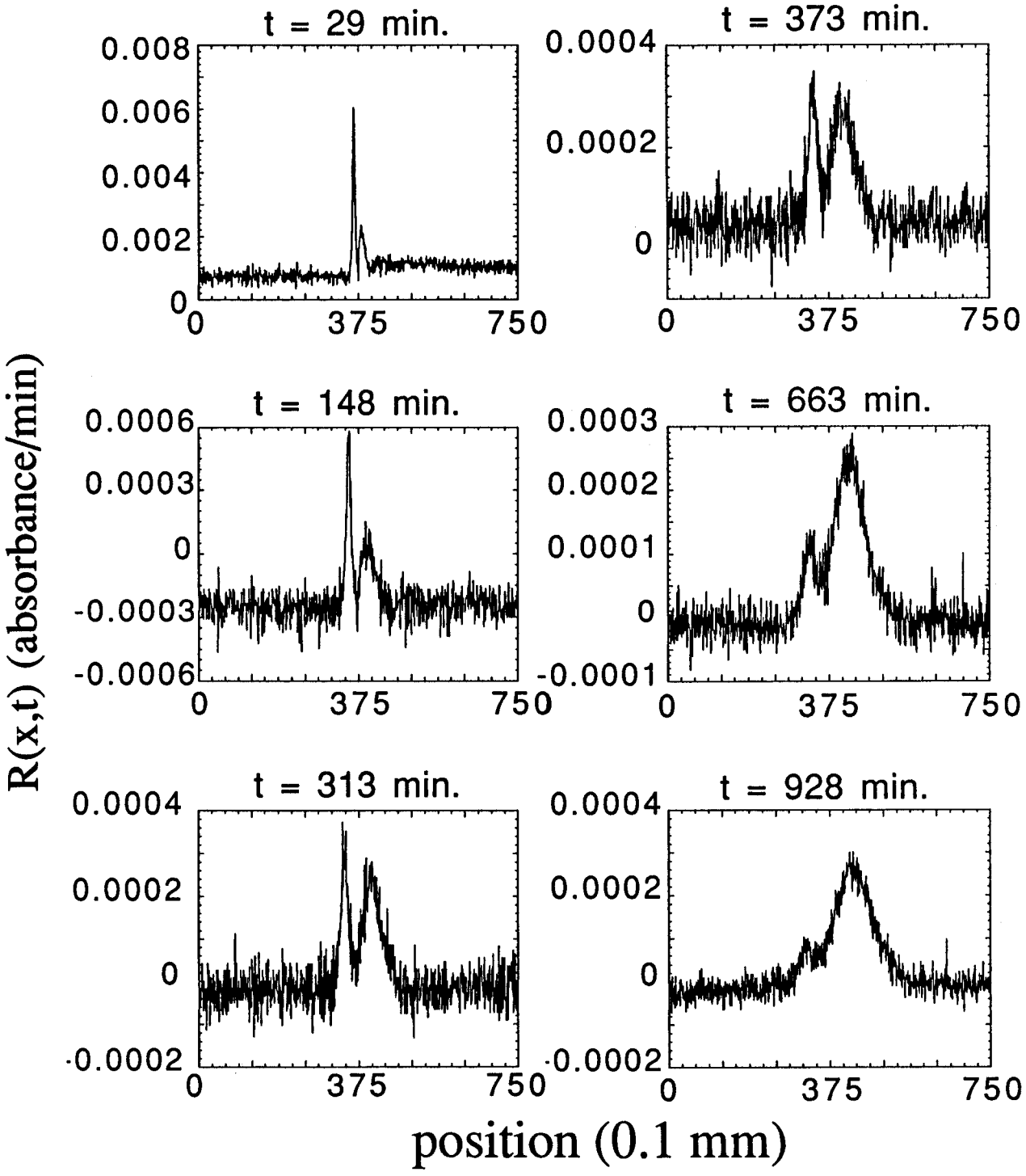

Figure 6. Experimental results for the reaction $R(x,t)$ vs position profiles at different times. Compare the splitting and evolution of the reaction fronts with Figure 10. Concentration of Cr^{3+} is 1.05×10^{-3} M and for xylenol orange is 1.1×10^{-4} M.

expected trend was indeed observed in a test tube containing a solution of Co^{3+}, instead of Cr^{3+}, with XO, under the same conditions as above. We note that Co^{3+} does not form oligomers in aqueous solution.[45] The reaction of Co^{3+} and XO proceeds faster at pH 4.5 compared to pH 4.0. As Co^{3+} does not aggregate in aqueous solution, the difference in reaction rate at pH 4.0 vs pH 4.5 is in this case due to the different XO ions in solution. In the case of XO reaction with Cr^{3+}, the effect of the k_i of the different XO species is overshadowed by those of the Cr^{3+} species. The effect of pH on the relative reaction rates reported above, for both the $Cr^{3+}-$XO and the $Co^{3+}-$XO reactions, were the same whether the reactant solutions were maintained at 100 or at 22 °C. Both reactions proceeded faster when heated.)

b. Reaction Front Kinetics. Figure 6 shows results for the temporal evolution of the spatial distribution of the product formation per time in terms of the change in absorbance, ΔA, over a time interval, Δt, versus position: $\Delta A/\Delta t$ vs x. We can see the splitting of the reaction front into two localized reaction fronts, starting at $t = 29$ min. As time progresses, the left peak diminishes while the right peak becomes the dominant peak in the $\Delta A/\Delta t$ vs x plot. Due to this splitting behavior we were unable to determine precisely the exponents for the width except

TABLE 1: Experimental Time Exponents [Theoretical Values in Brackets]

time regime	first	second	third	fourth
no. runs	4	5	3	4
$R(t)$	$+0.42 \pm 0.1$ [0.5]	-0.44 ± 0.1 [-0.5]	$+0.7 \pm 0.2$ [0.5]	-0.7 ± 0.2 [-0.5]
$w(t)$	$+0.50 \pm 0.05$ [0.5]	$+0.19 \pm 0.05$ [0.17]		

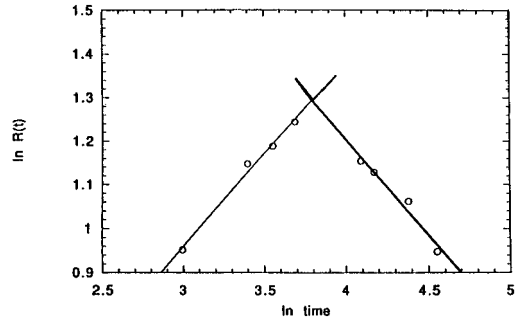

Figure 7. Log−log plot of global rate vs time. Notice crossover of the global rate exponent at early time from a positive slope of 0.42 to a negative slope of −0.44. Concentration of Cr^{3+} is 7.5×10^{-5} M and for xylenol orange is 5.0×10^{-4} M. The crossover time (t_{c1}) is at approximately 45 min. The errors in slope are about ±0.1.

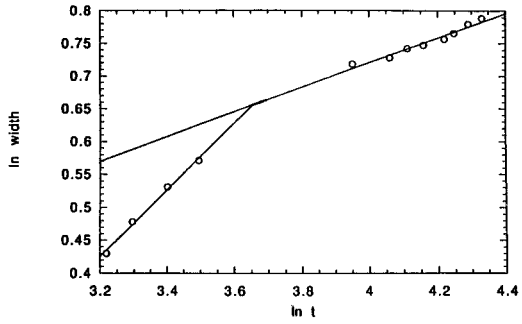

Figure 8. Log−log plot of width vs time. Notice the crossover of the width exponents at early time, from a slope of 0.50 to a slope of 0.19. Concentration of Cr^{3+} is 7.5×10^{-5} M and for xylenol orange is 5.0×10^{-4} M. The crossover time (t_{c1}) is at approximately 45 min. The errors in slope are about ±0.05.

at early times. However, we were still able to calculate the global rate, as shown below.

We measured the critical exponents of the global rate and of the width from log−log plots, shown in Figures 7 and 8, respectively, for the reaction of Cr^{3+} with XO. At early time, there exists a clear crossover of the scaling laws for both the width and for the global reaction rate. The first crossover time, t_{c1}, for both properties occurs at approximately 45 min.

Figure 7 shows the crossover of the global rate, from a $t^{0.42\pm0.1}$ behavior to a $t^{-0.44\pm0.1}$ behavior. Figure 8 shows the drastic early time crossover of the width behavior, from $t^{0.5\pm0.05}$ to $t^{0.19\pm0.05}$. That we were able to observe the early time behavior predicted for a single elementary reaction-limited reaction is to be expected, since at early times the fast reaction process dominates the kinetics. Effectively, at early time there is only one reaction contributing to the reaction front and the system exhibits the same early time behavior as a simple A + B → C reaction-diffusion system with initially separated reactants.[10−11] We note the reasonable agreement with the theory for both the global rate exponents and the width exponents (see Table 1).

Figure 9 shows the scaling of the global rate, which has more than one crossover in time, over the entire time scale of the experiment. No data were taken before $t = 15$ min, approximately, for this run, so for the early time crossover regime of the global rate, we refer to Figure 7. The first crossover time for the global rate is shown in Figure 7 and occurred at 45 min. The second and third crossover times for the global rate

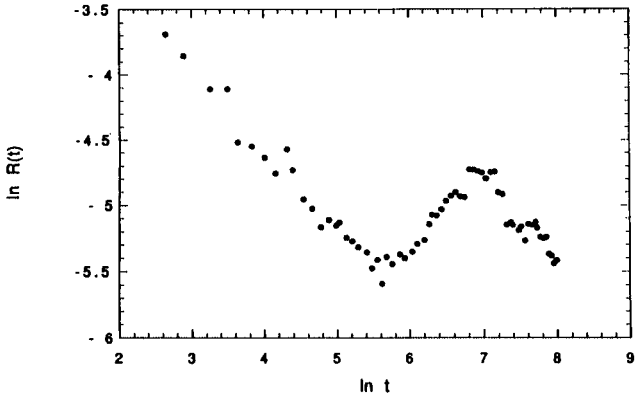

Figure 9. Experimental results for the global rate $R(t)$ as a function of time. More than one crossover observed. Concentration of Cr^{3+} is 1.05×10^{-3} M and for xylenol orange is 1.1×10^{-4} M. Compare with Figure 11.

occur at approximately 270 min and at approximately 1100 min, respectively.

The exponents for the different time regimes of the global rate and width behavior shown in Figures 7, 8, and 9 are summarized in Table 1. The experimental scaling exponents reported in Table 1 are the average slope values obtained from the log−log plots of several different runs of the experiment. Data obtained from both sets of the reactant concentrations reported in the experimental section contribute to the average values of the exponents reported here.

All three crossovers can be explained if one considers the conditions of the model for two competing reactions, one due to the chromium monomer and the other due to the higher order oligomers. The second crossover results from a "changing of the guard" of the fast reaction process and the slow reaction process—the negative slope (on a log−log plot of R vs t) of the fast reaction process, which dominates the global rate behavior at relatively early time, is overtaken by the slow reaction process, which begins its global rate ascent at later times. Because the reactant that contributes to the fast reaction has a much lower concentration, the fast reaction process eventually becomes negligible, and the slow reaction, which results from the high initial concentration reactant species, begins to dominate the reaction front behavior at later times. Eventually, the slow reaction process also crosses over, as the fast reaction process did, into its asymptotic, negative slope regime, causing the third crossover in time. Thus, the physics behind the third crossover is the same as for the first crossover, the only difference being that it occurs at a later time because it is a result of the slower of the two reaction processes. The marginal deviations of the experimentally determined exponents from the predicted exponents in the later time regimes may be due to the fact that the scaling theory pertains to a single elementary reaction process while the scaling exponents reported here result from the competition of two such processes. While these two competing processes are largely spatiotemporally resolved, they are still partially overlapped.

The first crossover time, from the early time to the late time behavior of the first, faster reaction process (due to the monomer) is shown in Figure 7 and occurred at $t = 45$ min. The second such crossover time, shown in Figure 9, resulted from the kinetics of the second, slower reaction process (due

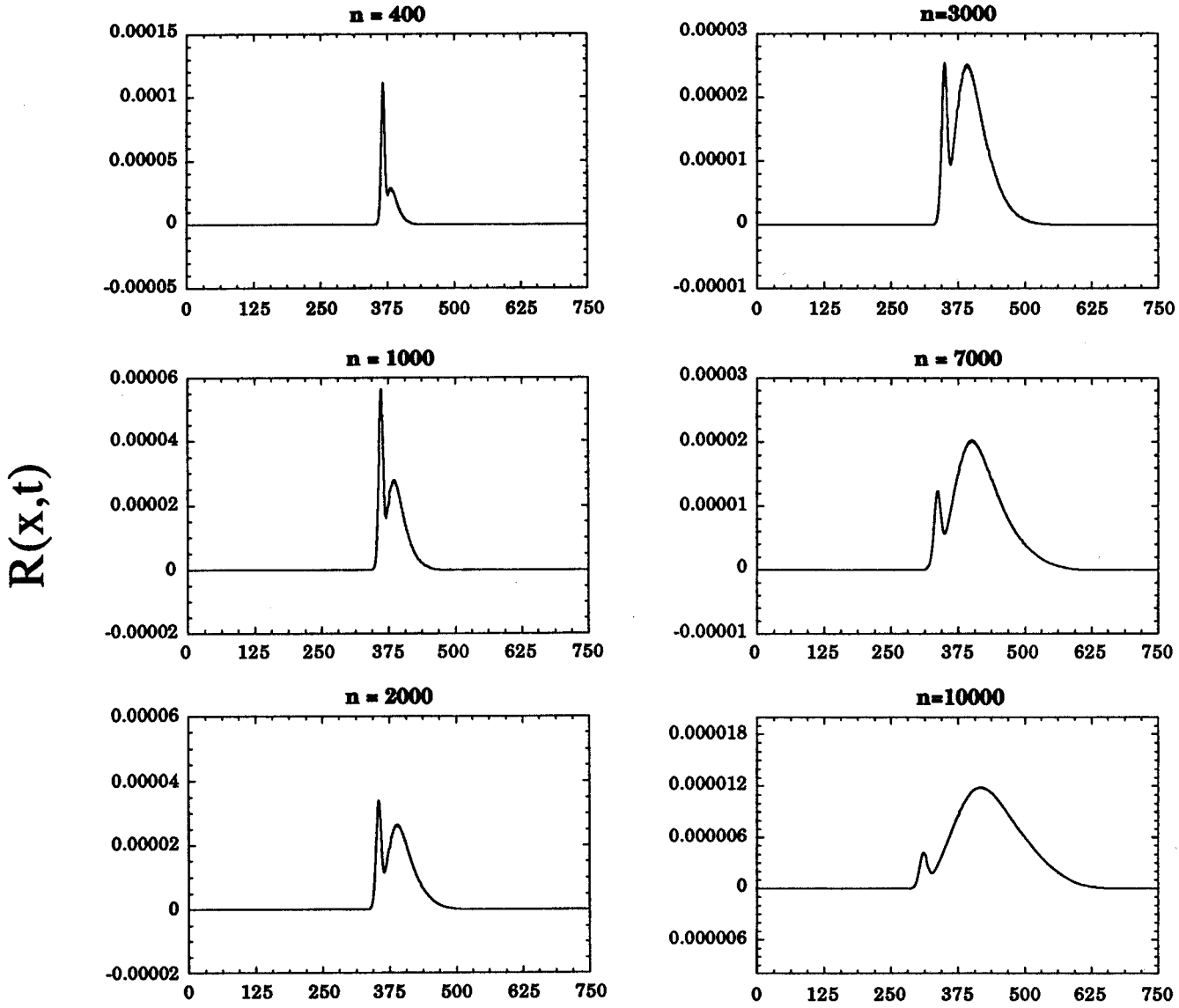

Figure 10. Numerical results for the time evolution of the spatial profile of the local production rate $R(x,t)$, for $k_1 = 1$, $k_2 = 10^{-4}$ and $a_1 = 3\%$, $a_2 = 97\%$ of total A density. Compare with experiment (Figure 6).

to the higher order oligomers) and occured at $t = 1100$ min. Note that Figure 9 does not show the early time crossover seen in Figure 7 for different initial concentrations. It has been predicted analytically[13] that the crossover time of the globalrate behavior, from the early time $t^{0.5}$ to the asypmtotic time $t^{-0.5}$, follows eq 6

$$t_c \sim \frac{C_0}{C_1 k (a_0 b_0)^{1/2}} \tag{6}$$

where t_c is the crossover time and C_0 and C_1 are constants. Thus, the crossover times observed in our experiments can be used to determine the relative rates of reaction for the two types of Cr^{3+} (monomers vs higher order oligomers) with XO. Taking into account the different initial concentrations used to obtain the results shown in Figures 7 and 9 (see appropriate figure captions), we calculate the relative rates of the two reactions to be $k_1/k_2 \cong 250$. We note that the chromium monomer concentration is about $0.03a_o$ and that of the oligomer is about $0.97a_o$ (see Figure 3). Significantly, the geometrical constraints and nonclassical behavior of the reaction rate enable us to extract this k_1/k_2 ratio.

In summary, it was shown that under conditions where k_1 and k_2 differ by several orders of magnitude, and where the faster reacting A_1 species is only a small fraction of the total density of A ($A = A_1 + A_2$), the reaction front splits in two. Futhermore, the global reaction rate is nonmonotonic in time, first increasing, then decreasing, then increasing again in time and finally decreasing asymptotically as $t^{-1/2}$, the same as the asymptotic behavior exhibited for the simple $A + B \rightarrow C$ elementary reaction.

c. Reaction Front Simulations. Figures 10 and 11 show simulation results for the reaction-diffusion system of two competing reactions with rate constants $k_1 = 1$ and $k_2 = 10^{-4}$ and initial densities $a_1 = 3\%$ and $a_2 = 97\%$ of the total A density. The inset figure in Figure 11 shows $R(t)$ vs t for the conditions $k_1 = 0.1$, $k_2 = 10^{-4}$ and $a_1 = 4\%$, $a_2 = 96\%$ of the total A density.

Figure 10 shows the spatiotemporal evolution of the product (P) formed over given time intervals, Δt: $R(x,t) \equiv \Delta P/\Delta t$ vs x. As can be seen, the experimental data and the simulation results are in excellent agreement with each other. The overall behavior is characteristic for a competition between a dilute, but fast reacting, component vs a concentrated, but slow reacting, component. Not shown are results for opposite relative reaction

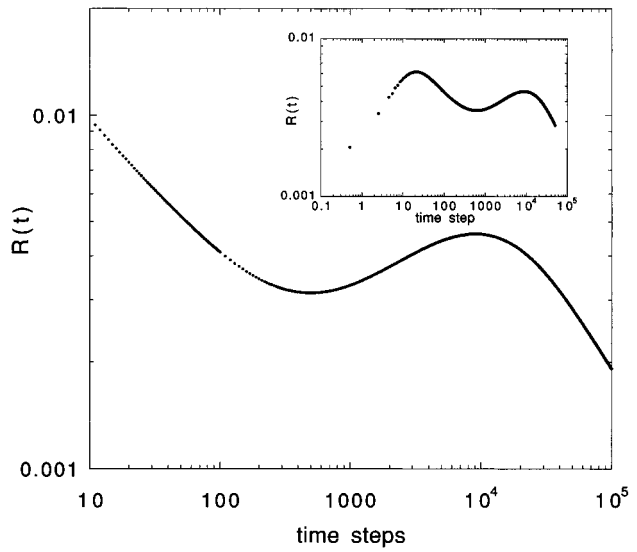

Figure 11. Numerical results of the global rate $R(t)$ as a function of time, for $k_1 = 1$, $k_2 = 10^{-4}$ and $a_1 = 3\%$, $a_2 = 97\%$ of total A density. Compare these results with experiment (Figure 9). The inset figure shows $R(t)$ vs t for the conditions $k_1 = 0.1$, $k_2 = 10^{-4}$ and $a_1 = 4\%$, $a_2 = 96\%$ of the total A density.

speeds, the contribution of the dilute component is mostly masked by that of the high-concentration component.

Figure 11 shows the temporal evolution of the global product rate, *R(t)*, obtained by integrating the superposition of the two processes over *x*, according to the scheme for competing reactions (eq 4). In the competing reaction system, the faster reaction, which is the main contributor to the global rate at early time, eventually begins to decay, while the slower reaction becomes the main contributor to the global rate of the system. The qualitative agreement between experiment and simulation is quite good, as can be seen by comparing Figures 9 and 11 and Figure 7 with the inset of Figure 11. However, the slope values of Figure 11 do not agree quantitatively with the slopes predicted by the analytical theories (Table 1), though still giving the correct trends (signs).

VI. Summary

We believe that the splitting of the chemical reaction front which we observed was the direct result of the reaction-diffusion kinetics of two competing reactions and that Cr^{3+} is the analog of the A_i species in our simulation model. For two competing reactions under initially separated conditions, where the major component reacts slowly and the minor component reacts quickly, we observed spatiotemporal patterns. Our experiment yielded spatial patterns similar to the ones generated from a computer model for this system of competing reactions. We observed at early time a crossover for both the global reaction rate and width, as predicted by perturbation theory for a simple $A + B \rightarrow C$ reaction, since the fast reaction dominates the early kinetics of the system. At later times, when the slower reaction begins to influence the kinetics, we observed front splitting and nonmonotonic behaviors of the global rate. At even later times we saw the slow component take over and exhibit the same rise and decline in rate as the fast component did earlier. From the ratio of the crossover times, corrected for initial concentrations, we are able to deterimine a value that expresses the relative reaction rates of the two competing reaction processes. The reaction probability of the chromium ion monomer is about 250 times greater than that of the average higher chromium ion oligomer. This information stems from the nonclassical rate laws encountered for such a low-dimensional reactor. As seen in the simple $A + B \rightarrow C$ case, the persistence of reactant segregation was also observed in the asymptotic regime for the competing reactions, where the slower reaction dominated, and, as a result, the global reaction rate decreased approximately with $t^{-0.5}$, the value predicted and observed experimentally for the asymptotic rate of the elementary $A + B \rightarrow C$ type reaction. All together, the global reaction rate crosses over twice from a reaction-limited $t^{0.5}$ slope to a diffusion-limited $t^{-0.5}$ slope. Overall, with no free parameters, the theoretical and simulation models are consistent with the complex spatiotemporal patterns and the unusual scaling laws observed experimentally. An interesting and self-consistent temporal pattern of scaling exponents and crossover behaviors has been documented.

Acknowledgment. We thank Dr. Steve Parus for help with the experimental design and Prof. Havlin for useful discussions. We appreciate support from NSF Grant No. DMR-9410709. R.K. also acknowledges support from the Guggenheim Foundation and the U.S.-Israel Binational Foundation, which enabled him to do some of the work at Bar Ilan University. H.T. acknowledges support by the Israel Science Foundation.

References and Notes

(1) Murray, J. D. *Mathematical Biology. Biomathematics*; Springer-Verlag: Berlin, 1993; Vol. 19.
(2) Avnir, D.; Kagan, M. *Nature* **1984**, *307*, 717 and reference cited therein.
(3) Lindenberg, K.; Romero. A. H; Sancho. J. M.; Sagues, F.; Reigada. R.; Lacasta, A. M. *J. Phys. Chem*. **1996**, *100*, 19066.
(4) Henisch, H. K. *Crystals in Gels and Liesegang Rings*; Cambridge University Press: Cambridge, 1988.
(5) Liesegang, R. E. *Naturwiss. Wochenschr*. **1896**, *11*, 353.
(6) Belouzov, B. P. *Khim. Zhizn*. **1982**, 7, 65. Zhabontinskii. In *Oscillating Processes in Biological and Chemical Systems*; Frank, G. M., Ed.; Science Publisher: Moscow, 1968.
(7) Ouyang, Q.; Li, R.; Li, G.; Swinney, H. L. *J. Chem. Phys*. **1995**, *102*, 2551.
(8) Toth, A.; Gaspar, V.; Showalter, K. *J. Phys. Chem*. **1994**, *98*, 522.
(9) Epstein, I. R.; Showalter, K. *J. Phys. Chem*. **1996**, *100*, 13132.
(10) Galfi, L.; Racz, Z. *Phys. Rev. A* **1988**, *38*, 3151.
(11) Koo, Y.-E. L.; Kopelman, R. *J. Stat. Phys*. **1991**, *65*, 893. Koo, Y.-E. L.; Li, L.; Kopelman, R. *Mol. Cryst. Liq. Cryst*. **1990**, *183*, 187.
(12) Jiang, A.; Ebner, C. *Phys. Rev. A* **1990**, *42*, 7483.
(13) Taitelbaum, H; Havlin, S.; Kiefer, J. E.; Trus, B.; Weiss, G. H. *J. Stat. Phys*. **1991**, *65*, S73.
(14) Taitelbaum, H.; Koo, Y-E. L.; Havlin, S.; Kopelman, R.; Weiss, G. H. *Phys. Rev. A* **1992**, *46*, 2151.
(15) Cornell, S.; Droz, M.; Chopard, B. *Physica A* **1992**, *188*, 322.
(16) Cornell, S.; Droz, M.; Chopard, B. *Phys. Rev. A* **1991**, *44*, 4826.
(17) Araujo, M.; Havlin, S.; Larralde, H.; Stanley, H. E. *Phys. Rev. Lett.* **1992**, *68*, 1791.
(18) Larralde, H.; Araujo, M.; Havlin, S.; Stanley, H. E. *Phys. Rev. A* **1992**, *46*, 855.
(19) Ben-Naim, E.; Redner, S. *J. Phys. A* **1992**, *25*, L575.
(20) Araujo, M.; Larralde, H.; Havlin, S.; Stanley, H. E. *Physica A* **1992**, *191*, 168.
(21) Havlin, S.; Araujo, M.; Larralde, H.; Stanley, H. E.; Trunfio, P. *Physica A* **1992**, *191*, 143.
(22) Havlin, S.; Araujo, M.; Larralde, H.; Shehter, A.; Stanley, H. E. *Fractals* **1993**, *1*, 405.
(23) Chopard, B.; Droz, M.; Karapiperis, T.; Racz, Z. *Phys. Rev. E* **1993**, *47*, R40.
(24) Cornell, S.; Droz, M. *Phys. Rev. Lett*. **1993**, *70*, 3824.
(25) Araujo, M.; Larralde, H.; Havlin, S.; Stanley, H. E. *Phys. Rev. Lett.* **1993**, *71*, 3592.
(26) Taitelbaum, H. *Physica A* **1993**, *200*, 155.
(27) Koo, Y.-E. L.; Kopelman, R.; Yen, A.; Lin, A. *MRS Symp. Proc.* **1993**, *290*, 273.
(28) Vilensky, B.; Havlin, S.; Taitelbaum, H.; Weiss, G. H. *J. Phys. Chem*. **1994**, *98*, 7325.
(29) Lee, B. P.; Cardy, J. *Phys. Rev. E* **1994**, *50*, R3287.
(30) Leyvarz, F.; Redner, S. *Phys. Rev. A* **1992**, *46*, 3132.
(31) Kopelman, R. *Science* **1988**, *241*, 1620 and reference cited therein.
(32) Taitelbaum, H.; Vilensky, B.; Lin, A.; Yen, A.; Koo, Y. E.; Kopelman, R. *Phys. Rev. Lett.* **1996**, 77, 1640.
(33) Yen, A.; Koo, Y. E.; Kopelman, R. *Phys. Rev. E* **1996**, *54*, 2447.
(34) Vilensky, B.; Taitelbaum, H. in preparation.

(35) Havlin, S.; Ben-Avraham, D. *Adv. Phys.* **1987**, *36*, 695.
(36) Koza, Z.; Taitelbaum, H. *Phys. Rev. E* **1996,** *54***,** R1040.
(37) Taitelbaum, H.; Yen, A.; Kopelman, R.; Havlin, S.; Weiss, G. H. *Phys. Rev. E* **1996**, *54*, 5942.
(38) Stunzi, H.; Spiccia, L.; Rotzinger, F. P.; Marty, W. *Inorg. Chem.* **1989**, *28*, 66.
(39) Snell, F. D. *Photometric and Fluorometric Methods of Analysis*; Wiley: New York, 1978; Part 1.
(40) Rehak, B.; Korbl, J. *Collection Czech. Chem. Commun.* **1960**, *25*, 797.
(41) Valci, O.; Nemcova, I.; Suk, V. *Handbook of Triarylmethane and Xanthene Dyes*; CRC Press: Boca Raton, FL, 1985.
(42) Burlatsky, S.; Ginzburg,V. V.; Clark, N. A. *Phys. Rev. E* **1996**, *54*, R1058.
(43) Cheng, K. L. *Talanta* **1967**, *14*, 875.
(44) Neurath, H. *Science* **1941**, *93*, 431.
(45) Pecoraro, V. Private communication, 1995.